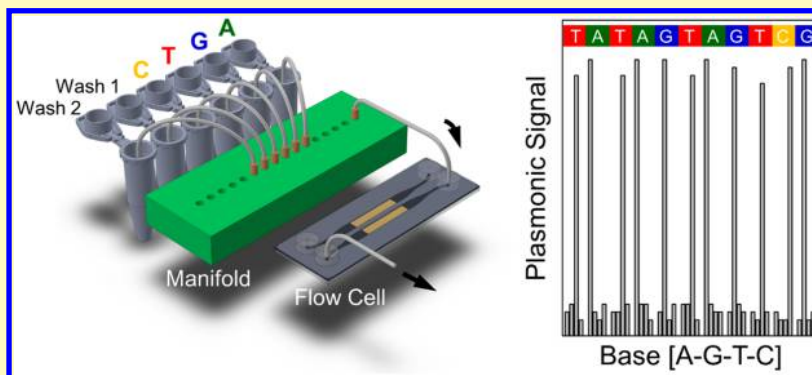


Plasmonic Sensor Could Enable Label-Free DNA Sequencing

Arif E. Cetin,^{*,†} Pinar Iyidogan,[†] Yuki Hayashi,[†] Mark Wallen,[†] Kandaswamy Vijayan,[†] Eugene Tu,[†] Michael Nguyen,[†] and Arnold Oliphant[†]

[†]Omniome, Inc., 10575 Roselle Street, San Diego, California 92121, United States

Supporting Information



ABSTRACT: We demonstrated a proof-of-principle concept of a label-free platform that enables nucleic acid sequencing by binding methodology. The system utilizes gold surfaces having high fidelity plasmonic nanohole arrays which are very sensitive to minute changes of local refractive indices. Our novel surface chemistry approach ensures accurate identification of correct bases at individual positions along a targeted DNA sequence on the gold surface. Binding of the correct base on the gold sensing surface triggers strong spectral variations within the nanohole optical response, which provides a high signal-to-noise ratio and accurate sequence data. Integrating our label-free sequencing platform with a lens-free imaging-based device, we reliably determined targeted DNA sequences by monitoring the changes within the plasmonic diffraction images. Consequently, this new label-free surface chemistry technique, integrated with plasmonic lens-free imaging platform, will enable monitoring multiple biomolecular binding events, which could initiate new avenues for high-throughput nucleic acid sequencing.

KEYWORDS: *plasmonics, label-free DNA sequencing, sequencing by binding, lens-free imaging, microfluidics, nanofabrication*

DNA sequencing technology is a key tool in a variety of fields, e.g., pharmacology, molecular biology, biotechnology, and genetics. Determining the sequence of the bases in DNA is very crucial for identifying genes associated with diseases,^{1,2} developing personalized drugs,^{3,4} monitoring gene mutations for cancer research,^{5,6} and understanding gene functions.^{7,8} Numerous advancements have been made in sequencing technologies based on detecting incorporation of fluorescent nucleotides,^{9,10} ligation of fluorescent oligonucleotides,^{11,12} release of pyrophosphate,^{13,14} release of protons,^{15,16} and passage of DNA or other synthesis byproducts through protein nanopores.^{17,18} Despite progress in DNA sequencing technology and the growing importance of nucleic acid sequencing information, further developments are needed to reduce the cost, increase the read-length, and improve data quality.

The development of high-throughput sequencing platforms, namely, next generation sequencing (NGS), has been driven by the high demand for cost-effective sequencing. Massively parallel techniques allow millions of sequences to be determined with just a single sequencing run. The development of fluorescence-based sequencing methods dramatically reduced the complexity of obtaining large amounts of sequencing

data, while improving the speed. Currently, there are several commercially available fluorescence-based NGS platforms employing different techniques. For example, Solexa/Illumina sequencing subjects an array of DNA clusters to serial polymerase-catalyzed extension steps using nucleotides that are fluorescently labeled with different colors, and the sequence of each cluster is determined from serial images of the array after each extension step.^{19,20} In addition, SOLiD sequencing employs an array of amplicons on beads that are subjected to serial ligation of fluorescently labeled oligonucleotide probes and the sequence on each bead is determined from serial fluorescent images of the beads.²¹ Although these methods significantly improved the throughput, they suffer from problems related to the use of labels such as the complexity and the high cost of labeling processes, mismatch between number of fluorescence dyes and nucleotides, photobleaching issues, or the need to modify components within the reaction to accommodate the bulk of the fluorescent label.

Received: December 23, 2017

Accepted: February 28, 2018

Published: February 28, 2018

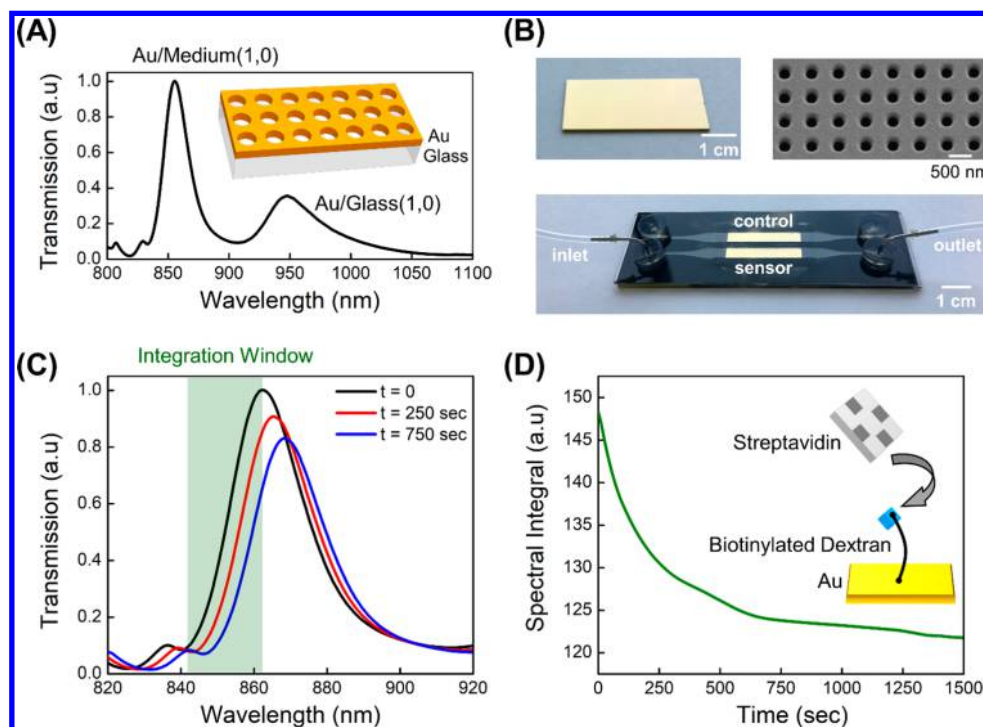


Figure 1. (a) Transmission response of the nanohole array under deionization water. Schematics shows the nanohole array realized through thin gold film on a glass substrate. Hole diameter: 200 nm, array periodicity: 600 nm, and gold film thickness: 120 nm. (b) Top-left: Photograph of the plasmonic sensor chip. Top-right: SEM picture of the nanohole array. Bottom: Photograph of the flow cell composed of a double-channel microfluidic chamber and a plasmonic sensor chip. (c) Transmission response of the nanohole array at different time points upon the delivery of streptavidin. The green rectangle is the spectral window where the light transmissions at each wavelength are integrated. (d) Spectral integration variation in real-time upon the attachment of streptavidin on the dextran-coated gold nanohole surface.

Recently, plasmonic sensor platforms have received significant attention as they allow label-free biodetection thanks to their high sensitivities to even minute biomolecular concentrations via allowing strong light/matter interactions.^{22,23} In these platforms, the presence of biomolecules on the plasmonic surface can be detected by monitoring the spectral variations in their optical responses without the need for any fluorescence tag.²⁴ Earlier, we introduced a label-free DNA sequencing platform based on surface plasmon resonance (SPR), which provides the sequence data without the need for any label.²⁵ The system utilizes a prism-coupling mechanism integrated to a gold sensor film, where the nucleotides are delivered to the gold sensing surface via a fluidic chamber. Since gold is a highly biocompatible material, SPR sensors ensure robust surface chemistry and functionalization, enabling target-specific detection. Even though our SPR sensor technique provides accurate sequence data thanks to its ultrasensitive nature, it is limited in multiplexing and throughput due to its alignment sensitive prism coupling scheme. Recently, plasmonic structures consisting of nanoparticles or nanoapertures have been proposed due to their extraordinary light confinement and field enhancement capabilities.^{26–29} Particularly, platforms utilizing periodic nanohole arrays support extraordinary light transmission (EOT) through the unique integration of localized surface plasmon modes of the apertures and the propagation surface plasmons excited by the grating order of the array.³⁰ In addition to their ultrasensitive responsiveness to minute change in the local refractive index, like SPR platforms, the grating coupling mechanism in nanohole arrays enables plasmonic excitations even at normal incidence. This collinear configuration also makes these aperture platforms an ideal candidate

for high-throughput sensing applications by integrating them to imaging based devices.^{31–35}

In this letter, we introduce a nucleic acid sequencing platform that employs sequencing by binding (SBB) methodology³⁶ in a label-free detection device. The platform achieves sensitivity using gold nanohole arrays that support plasmonic resonances, which are highly sensitive to change in the local refractive index. We employed a thiol based surface chemistry, which yields a robust attachment of DNA templates to the sensing surface and allows correct base-pairing for protein complexes formed on the templates. SBB methodology detects the binding of nucleotide-specific complexes. In essence, the method slows the incorporation process. Immediately before the incorporation of the nucleotide, a complex consisting of the primer-template, polymerase, and the correct nucleotide is formed. The SBB methodology stops the incorporation process at this point to detect the formation of this complex. With the versatile SBB method, detection can be facilitated by labeled nucleotides and/or labeled polymerase, but labels need not be used. Formation of protein complexes on the sensing surface triggers a spectral shift within the plasmonic modes supported by the nanohole arrays, and accurately identifies the correct sequence of different DNA templates with high signal-to-noise ratio (SNR). Combining the sequencing platform with an imaging based system, we monitored protein complex formations via the diffraction intensity variations observed in plasmonic lens-free images. We believe that in the future our lens-free technique could pave the way for a high-throughput and label-free sequencing platform by allowing the entire sensor surface to be utilized for multiple sequencing applications.

In our label-free platform, SBB methodology exploits the specificity with which a protein complex will form between a primed-template DNA, a correct nucleotide, and a polymerase, without necessarily incorporating the next nucleotide. Each cycle of the SBB method generally includes steps of (a) contacting a primed-template DNA with a polymerase and a known nucleotide under conditions that preclude primer extension; (b) detecting the complex that is formed; and then (c) extending the primer by a single nucleotide to step to the next position of the template. The cycle can be repeated to identify the series of nucleotides that correctly complement sequential positions along the template, thereby elucidating the sequence of the template. An advantage of SBB methodology is that, although detection can be facilitated by labeled nucleotides and/or labeled polymerase, labels need not be used to observe protein complexes and thus determine template sequences.

RESULTS AND DISCUSSION

Label-free identification of targeted DNA sequences is realized through a plasmonic sensor chip, composed of a periodic nanohole array realized through a 120-nm-thick gold film on a fused silica (glass) substrate. Figure 1a shows the transmission response of the nanohole array with 200 nm hole diameter and 600 nm periodicity under deionization water (see Experimental Section for the spectroscopic analysis). Here, we observed two transmission resonances at ~ 855 nm and ~ 949 nm, where the former one is due to the SPP excitations at the gold–water interface, e.g., Au/Medium (1,0) mode, and the latter one is due to the SPP excitations along the interface between the gold and glass layers, e.g., Au/Glass (1,0) mode.³² The transmission resonance at shorter wavelengths extends deep into the surrounding medium so that it is more exposed to the change in the local refractive index compared to the resonance at longer wavelengths as it is trapped between gold–glass interface (see Experimental Section for the physical origin of the two plasmonic modes).¹⁰ Therefore, we focused on the spectral variations within the Au/Medium (1,0) mode for our sequencing experiments. The sensor chip is realized through a high-throughput and overlage area fabrication method based on deep-UV lithography (see Experimental Section for the details of the fabrication method).^{33,34} Figure 1b, top-left, shows the photograph of the 25 mm \times 13 mm sensor chip, where the nanohole apertures are fabricated over the whole gold surface. Figure 1b, top-right, shows the scanning electron microscope (SEM) image of the nanohole array demonstrating the quality of our fabrication method. For our real-time SBB experiments, we utilized a flow cell composed of the plasmonic sensor chip integrated with a double-channel microfluidic chamber, serving as sensor and control as shown in Figure 1b, bottom (see Experimental Section for the details of the flow cell). Here, the control channel is used to eliminate any optical, mechanical, or chemical fluctuations. Figure 1c shows the transmission response of the nanohole array at different times upon the attachment of 25 nM streptavidin (Sigma-Aldrich) that is delivered to the sensing surface with a 5 $\mu\text{L}/\text{s}$ flow rate. Here, the gold surface is spin-coated with biotinylated dextran (Molecular Probes). Transmission response of the nanoholes coated with biotinylated dextran (black curve) at ~ 862 nm shifts to ~ 865 nm and ~ 868 nm by 250 s (red curve) and 750 s (blue curve), respectively, after the delivery of streptavidin. In order to reliably monitor the spectral variations due to the attachment of the targeted analytes to the sensing surface, we

used a spectral integration method instead of focusing only on the changes within the resonance wavelength of the transmission resonance. Doing this, we were able to collectively contribute spectral variations within multiple wavelengths, which dramatically improves the detection limit to sense minute spectral variations in the presence of low concentrations of biomolecules.³² Here, we integrated the transmission values at each wavelength within the spectral window highlighted with green rectangular box in Figure 1c. Figure 1d shows the spectral integral value over time, where the integral value dramatically decreases due to the mismatch between the nanohole transmission response and the spectral window upon the attachment of streptavidin, triggering spectral shifts within the transmission resonance. This result demonstrates the ultra-sensitive character of our sensing platform to minute changes within the local refractive index triggered by the presence of the targeted analytes, which allows monitoring the molecular binding kinetics in real-time.

Figure 2 shows the schematics of the surface chemistry method that enables label-free SBB methodology. The gold

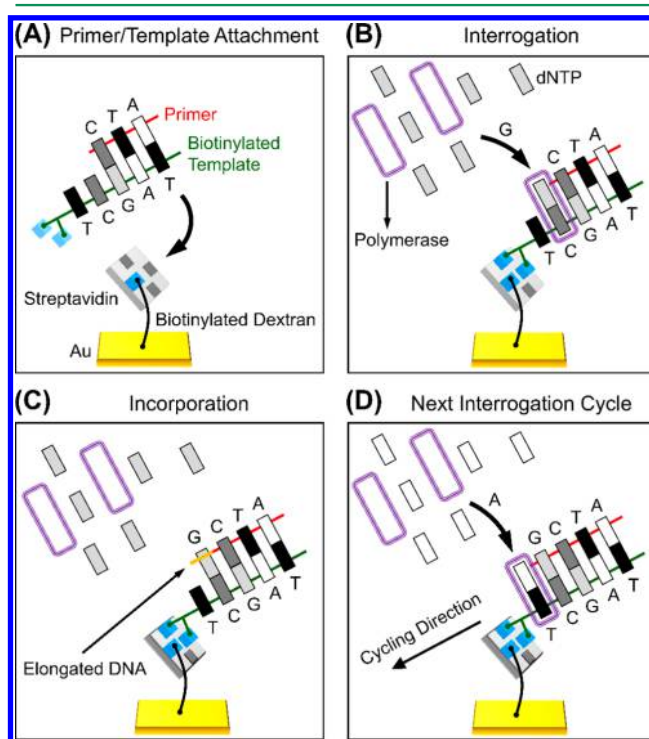


Figure 2. Sequencing by binding chemistry enabling label-free DNA sequencing. (a) Biotinylated primer-template binds on the gold surface through the biotin–streptavidin complex. (b) Polymerase ensures the correct dNTP–template pairing. (c) Complexes are stripped from the primed template followed by an incorporation step, where the correct dNTP is incorporated, and the primer is elongated. (d) The next cycle starts with the flow of the interrogation reagents. Figure illustrates the cycling direction.

sensor chip is first cleaned with a piranha solution (sulfuric acid [Sigma-Aldrich] and hydrogen peroxide [Honeywell-Fluka] composition) in order to eliminate any biological contamination. Biotinylated dextran is spin-coated on the gold surface and 25 nM streptavidin is flowed over the sensing surface. This ensures a strong capturing mechanism to specifically target the biotinylated primer-template. As illustrated in Figure 2a, a biotinylated primer-template is introduced to the sensing

Table 1. Primer and Template Sequence List^a

Oligo Name	Primer/Template	Sequence
FP1	Primer	5'- GAAGAGGAGTCTCTCAGCATAACGATACCACTGA -3'
GC50-A	Template	CGATTATCACGTTTACGCGGCGTGTATTCCTCAAGGTGAAGGCC GAACTACTATATCAGTGGTATCGTTATGCTGAGGACTCCTCTTC
FP2	Primer	GAGGGTCAGTGGTATCGTT
PhiX100	Template	GCAAATCACCAGAAGCGGTTCTGAATGAATGGGAAGCCTTCAA GAAGGTGATAAGCAGGAGAAACATACGAAGGCGCATAAACGATAC CACTGACCCTC

^aRed/Green: Primer/Template Pair. Blue: Sequence to be determined from right to left.

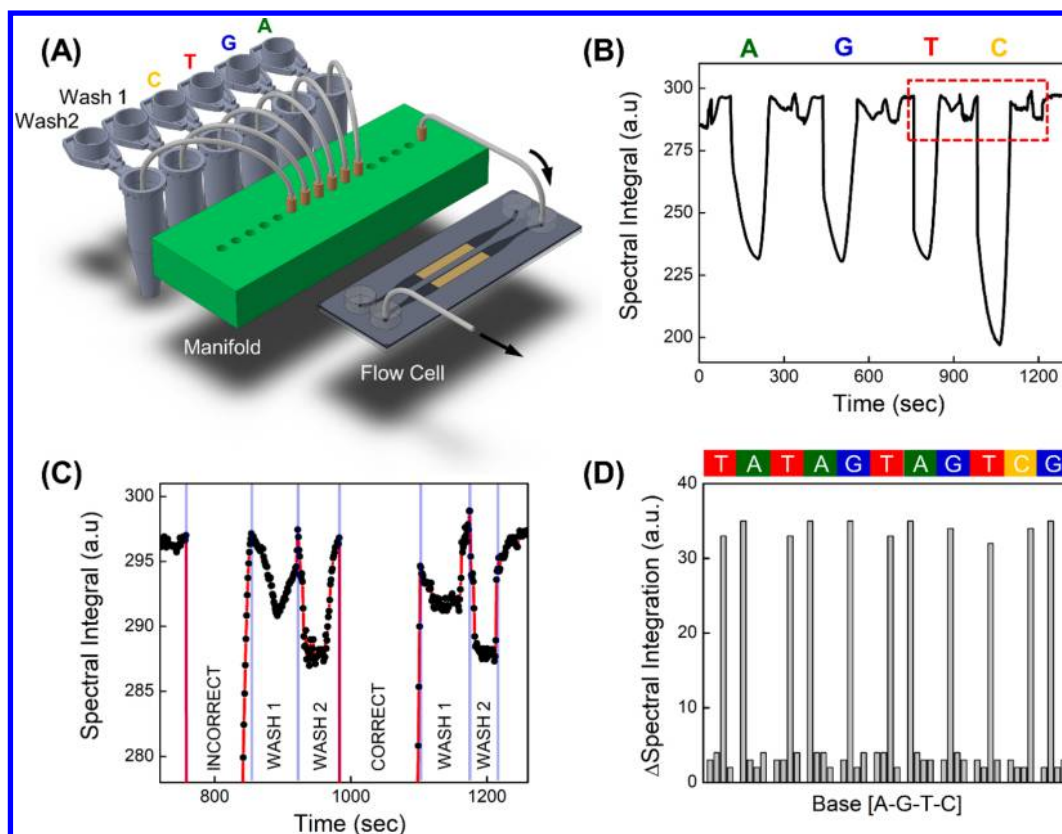


Figure 3. (a) Schematics of the fluidic platform composed of a manifold and a flow cell. (b) Spectral integration vs time for a sequencing cycle consisting of 4 bases for GC50-A primer template (Correct base: C). (c) Zoom image of two interrogation steps (shown with a red dashed box in Figure 3b) demonstrating the steps of a sequencing cycle, triggering spectral variations within the transmission resonance. In order to show the whole sequencing steps in detail, integral values corresponding to the interrogation steps are not fully shown. (d) Change in the spectral integral value for 11 sequencing cycles, where each cycle consists of 4 interrogation steps in the order of A, G, T, and C.

surface, which attaches through biotin and streptavidin interactions. In this article, we studied two templates, GC50-A (Integrated DNA Technologies, Inc.) and PhiX100 (Integrated DNA Technologies, Inc.) as shown in Table 1. Each sequencing cycle includes the following steps: (i) interrogation by contacting the primer-template with DNA polymerase and one of four native dNTPs to investigate under conditions that allow polymerase-DNA-dNTP complex formation but inhibit polymerase primer extension activity, (ii) removal of polymerase from the primed template, and (iii) incorporation of the correct nucleotide to the 3' end of the primer. Each sequencing cycle was started with equilibration of the surface with interrogation buffer without any polymerase and nucleotide, and followed by the same buffer including one of the nucleotides and polymerase to determine whether a protein complex was formed consisting of polymerase, dNTP, and template. The interrogation steps involved flushing the

primer-template derivatized surface with an interrogation buffer that contains a proprietary DNA polymerase that will not incorporate nucleotides and 100 nM of one type of deoxynucleotide triphosphate (dNTP) solution (Figure 2b illustrates an interrogation cycle for a correct base). Our interrogation was carried out in four sequential steps, each step including fluidic delivery of polymerase and a different nucleotide type (the order was dATP, dGTP, dTTP, and dCTP) and each step including detection of any complex formed. After each interrogation cycle the protein complex was removed and the surface was prepared to start the next nucleotide interrogation cycle. After performing a total of four interrogation cycles with one correct and three incorrect bases, an incorporation buffer containing a fully functional polymerase and 100 nM dNTP was flushed (Figure 2c) to incorporate the next incoming correct base. In this proof-of-principle demonstration, the base-specific incorporation buffer is

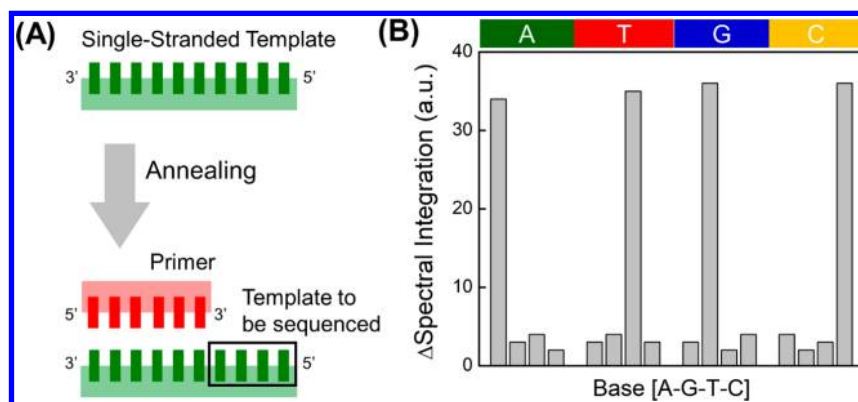


Figure 4. (a) Annealing for preparing primer/template pair. (b) Change in the spectral integral value for 4 sequencing cycles on PhiX100 template, where each cycle consists of 4 interrogation steps in the order of A, G, T, and C.

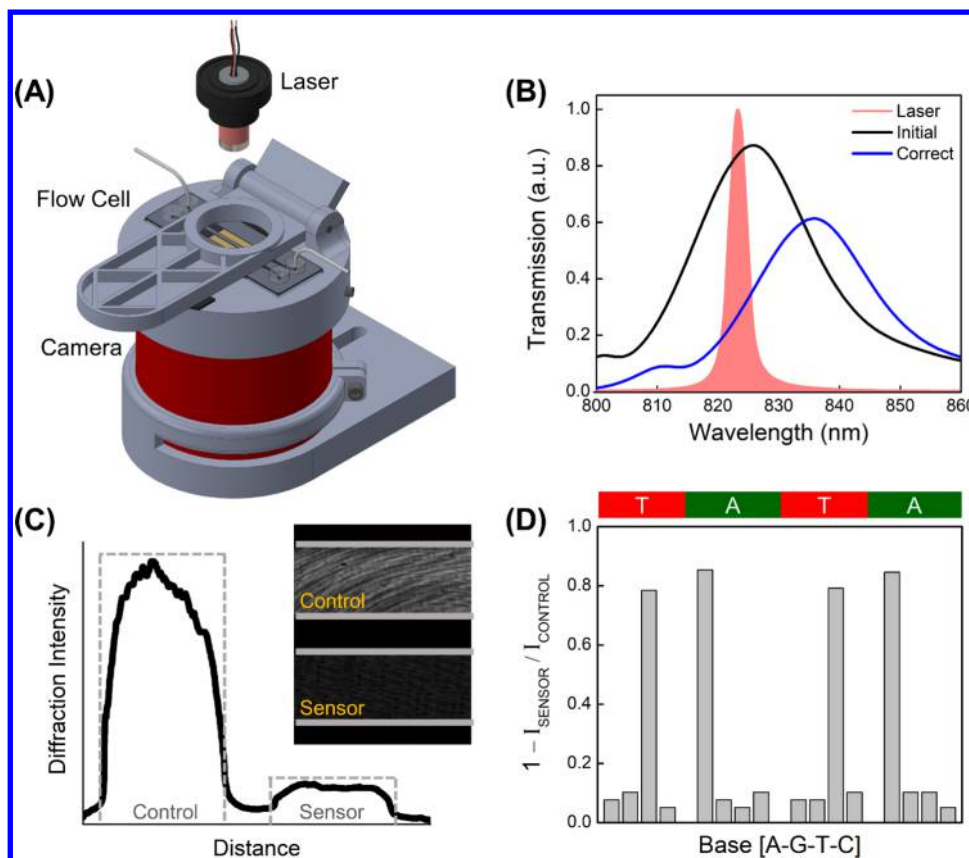


Figure 5. (a) Schematics of the imaging based label-free DNA sequencing platform, employing a laser diode, a fluidic chamber, and a CMOS camera. (b) Transmission response of the laser source, and that of the nanohole arrays before and after the binding of the correct base. (c) Diffraction intensities of control and sensor channels with the correct base interrogation in cross section. Figure inset is the real picture of the diffraction images of control and sensor channels. (d) Change in the intensity of the diffraction patterns ($1 - I_{\text{SENSOR}}/I_{\text{CONTROL}}$) for the first 4 bases of the GC50-A template.

introduced at the end of four cycles and chosen based on the base giving the highest signal change (correct base). The surface was cleared from any formed protein complexes and the next cycle (Figure 2d) was started with a flow of the interrogation reagent.

Figure 3a shows the schematics of our fluidic platform, composed of a manifold for the base selection and a flow cell which consists of a double-channel microfluidic chamber and the plasmonic sensor chip (see Experimental Section for the details of the complete setup). Figure 3b shows one sequencing cycle (correct base: C), starting with a washing step, followed

by 4 interrogation steps of bases in the order of A, G, T, and C. The figure clearly demonstrates the dramatic decrease within the spectral integral value due to the formation of a protein complex with the correct base, C, on the sensing surface, while the incorrect bases show smaller drops in the spectral integral value (only due to polymerase binding) due to the lack of correct base binding (see Supporting Figure 5 for the spectral integral change due to the attachment of polymerase to the sensing surface). Figure 3c zooms into the time window highlighted with a red dashed box in Figure 3b, (interrogation steps: T, C and correct base: C), demonstrating the spectral

variations within the nanohole transmission resonance triggered by the sequencing steps. This result indicates the ultrasensitive nature of our platform for real-time monitoring of biomolecular binding kinetics. We employed a template, GC50-A (Table 1) with FP1 Primer (Table 1). Figure 3d shows the change in the spectral integral value due to the formation of protein complexes for 11 sequencing cycles. The corrected signal level is calculated by subtracting out the signal change due to polymerase binding, which is determined by using a control channel. We successfully predicted the correct bases using the corrected signal levels. The spectral variation value due to the incorrect bases is negligible. The correct base yields approximately 1 order of magnitude larger integral value change compared to the incorrect bases. This distinct signal difference between correct and incorrect interrogation steps demonstrates the reliability of our label-free sensing platform for sequencing applications.

We investigated another template to further demonstrate the accuracy of our label-free sequencing platform for predicting the correct bases in a particular sequence. As shown in Figure 4a, the single-stranded DNA templates are annealed (GeneAmp PCR system 9700) with the corresponding primer to attach to the template. Here, we utilized PhiX100 Template (Table 1) and FP2 Primer (Table 1). Figure 4b shows the change in the spectral integration value due to the attachment of each base in the order of A, G, T, C. The figure demonstrates the successful prediction by our label-free sequencing platform for the first 4 bases, where the correct base yields approximately 1 order of magnitude larger integral value change compared to the incorrect bases.

As the transmission resonance of the nanoholes carries intensity information, they can be detected by an imaging device, i.e., a complementary metal–oxide semiconductor (CMOS) camera (see Experimental Section for the details of the lens-free platform).³⁵ By integrating nanohole sensors to a CMOS camera, multiple binding events can be monitored, which could dramatically improve the throughput. As a first step of the demonstration of label-free identification of targeted DNA sequences through an imaging based plasmonic system, we utilized a lens-free platform, composed of (i) a laser diode source (dominant wavelength at ~ 823 nm) which spectrally overlaps with the transmission resonance of the nanoholes, (ii) a flow cell, composed of a double-channel microfluidic chamber and a plasmonic sensor chip, and (iii) a CMOS camera to detect the diffraction patterns of the plasmonic response (Figure 5a). Figure 5b shows the laser response (dominant wavelength: ~ 823 nm), and the nanohole transmission response before (at ~ 826 nm, black curve) and after (at ~ 833 nm, blue curve) the correct base interrogation. In this configuration, the nanohole chip acts like a bandpass filter. When the nanohole transmission resonance matches with the laser response, it allows the maximum number of photons to pass through. When a protein complex containing the correct bases is present, it will bind to the sensing surface, thus shifting the transmission resonance to longer wavelengths. With the transmission resonance no longer matching the laser response, the number of photons reaching the CMOS detector decreases drastically. Figure 5c shows the intensity of the plasmonic diffraction patterns of the two microfluidic channels reserved for the control and the sensor (intensity profile is determined along the distance normal to the microfluidic channels). The figure demonstrates the dramatic reduction in the intensity of the diffraction pattern in the sensor compared to control due to

the binding of the protein complex to the sensing surface, triggering a spectral shift in the nanohole transmission response. The total transmission (intensity of diffraction patterns) for each sensor is calculated by summing the pixel photon count values over an area of $500 \mu\text{m} \times 500 \mu\text{m}$. Figure 5d shows the ratio between the diffraction pattern intensity of control and sensor ($1 - I_{\text{SENSOR}}/I_{\text{CONTROL}}$) for the first 4 bases of GC50-A template, demonstrating the dramatic signal difference between correct and incorrect bases. This result successfully proves the accuracy of our imaging based label-free DNA sequencing method. Our initial results with plasmonic lens-free images prove that screening the entire sensing surface for biomolecular binding events could be done through label-free plasmonic platforms. In the future, these platforms could be used to sequentially evaluate multiple sequencing events all in the same platform, which could open doors for high-throughput and label-free DNA sequencing.

Our results provide a “proof-of-principle” demonstration of identification of targeted nucleotide sequences and prove the feasibility of label-free, multiplexed, and high-throughput DNA sequencing. In this section, we will talk about future approaches for improvements on optics, nanochip technology, and surface chemistry for increasing the throughput, accuracy, read-length, and sequencing speed, while lowering the reagent consumption. We will investigate simultaneous sequencing of different primer templates for multiplexed sequencing and high-throughput sequencing of the same template for improving reliability of the sequencing information. This will be facilitated by the development of new surface chemistry methods, e.g., to isolate a large number of different or identical primer templates on the same surface. Understanding of the kinetics of the SBB chemistry will allow improvements in the binding efficiency of bases to primer template to achieve shorter interrogation duration (high sequencing speed), yielding more sequence data in the same amount of time. Furthermore, the ability to evaluate nanohole response of smaller arrays for sequencing will provide a path to significant improvements in throughput as the whole sensor chip surface could be utilized for multiple sequencing experiments. For this, methods to increase the transmission efficiency of small aperture arrays as well as to utilize high-intensity light sources for strong plasmonic diffraction intensities will be important to investigate. In addition to transmission efficiency, for the selection of the array size, the line-width of the transmission resonances will also be considered. The creation of robust image processing techniques that differentiate intensity information for each interrogation step under the presence of low diffraction intensities of smaller arrays will also be crucial. We expect the principles demonstrated on this label-free, plasmonic SBB platform to be transferrable to a variety of other sensing platforms including those that detect labels added to the nucleotides and/or polymerase.

CONCLUSION

In conclusion, we introduced a proof-of-principle demonstration of a sequencing platform utilizing sequencing by binding (SBB) methodology not requiring additional labels for detection. The platform employs a plasmonic surface having nanoholes through thin gold film with strong transmission resonances that are highly sensitive to local refractive index variations. The platform accurately provides targeted sequence data by detecting protein complexes formed by polymerase mediated pairing of a correct nucleotide with a primed-template

DNA on the sensing surface resulting in spectral variations within plasmonic transmission resonances. We further developed our sequencing platform by integrating it with an imaging based device. In our lens-free platform, we provided the sequencing data by monitoring the intensity variations within the plasmonic diffraction patterns due to the formation of protein complexes on the sensing surface. As it enables the utilization of the whole sensing surface for sequencing, our lens-free platform is an ideal candidate for low-cost, high-throughput label-free DNA sequencing applications.

EXPERIMENTAL SECTION

Spectroscopic Analysis. Transmission response of the nanohole arrays were determined by an Ocean Optics USB2000+ spectrometer fiber coupled to Zeiss Axiovert 200 M inverted microscope. We utilized a normally incident broadband halogen lamp. The spectral variations were calculated by a custom-made RStudio code, where the experimental data was smoothed by Savitzky-Golay filter.

Nearfield Properties of Plasmonic Modes. Supporting Figure 1a,b shows the amplitude of the y -component of the magnetic field (the dominant component for an x -polarized light source) at the gold–water interface (top surface of the Au film) for the Au/Medium mode and at the gold–glass interface (bottom surface of the Au film) for the Au/Glass mode, respectively. Here, the symmetric standing field patterns along the x -direction are due to two counterpropagating surface plasmons and hot spots along the y -direction are due to the localized surface plasmons. Hence, the transmission resonance of the nanoholes is excited through the unique integration of localized and propagating surface plasmons. The total electric field intensities calculated at the top surface of the Au film for the Au/Medium mode and at the bottom surface of the Au film for the Au/Glass mode are shown in Supporting Figure 1c,d, respectively, which are maximum at the rims of the nanoholes along the polarization direction (x -polarization). For the Au/Medium (1,0) mode, electric field intensity calculated along the xz -cross section at the nanohole rims shows that local electromagnetic fields concentrate at the top gold surface (Supporting Figure 1e), while for the Au/Glass (1,0) mode, they concentrate at the interface between gold film and glass layer (Supporting Figure 1f). As for the Au/Medium mode, the local fields extend deep into the surrounding medium, while they are trapped at the gold–glass interface for Au/Glass mode, the Au/Medium (1,0) mode is more sensitive to changes in the local refractive index, making it a better candidate for sensitive sensing applications.

Fabrication of Nanoholes. Plasmonic nanohole chips were obtained from the University of California, Santa Barbara (UCSB) Nanofabrication Facility. Supporting Figure 2 shows the fabrication steps: (i) 120 nm Au and 5 nm Ti were deposited on a 4 in., 500- μ m-thick fused silica wafer. (ii) Deep-UV lithography was performed on the photoresist coating the whole wafer surface. (iii) The photoresist was developed, and the metal film was etched by ion beam milling. (iv) The remaining photoresist was removed by oxygen plasma cleaning. This fabrication method allows the realization of the subwavelength nanoholes over the whole wafer surface. Finally, the wafer was diced in order to realize plasmonic sensor chips with a dimension of 25 mm \times 13 mm.

Assembly of Flow Cell. Supporting Figure 3 shows the multilayer structure of the disposable flow cell composed of a double-channel microfluidic chamber and a plasmonic sensor chip. The patterns are realized with a cutting plotter (Silhouette Cameo). Layer (iii) is a sheet of Zeonex cyclo-olefin polymer lined with a double-sided tape on the bottom, with a total thickness of \sim 0.5 mm. Layer (iv) is a black vinyl tape with a rubber based adhesive. Layer (v) is a double-sided pressure sensitive adhesive with an acrylic based adhesive and a polyester carrier, with a total thickness of 175 μ m. Layer (vi) is a cyclic olefin copolymer microscope slide with a 250 μ m thickness. The rectangular frame (iii) with a cavity with the size of the plasmonic sensor chip (ii) stabilizes the chip on the microscope glass slide (i). Layer (vi) seals the top of the microfluidic chamber and contains the

inlet and outlet holes. The press-fit tubing connectors from Grace Biolabs (vii) were used to seal and secure the fluidic connections attached to the microfluidic chamber. The structure of the microfluidic chamber is defined by the shape of the cavity on the pressure sensitive adhesive (v) and the black vinyl tape (iv) is used to occlude parts of the plasmonic sensor chip from the laser above, thereby eliminating background noise and minimizing the sensing volume.

Fluidic Setup. Supporting Figure 4 shows the fluidic setup. The microfluidic platform employs a Tecan Cavo XLP6000 syringe pump and is driven by negative pressure. The selection of reagents is made via multiple subminiature pneumatic cylinders (SM-2 subminiature cylinder from Clippard) and solenoid valves (Manifold VV100-S41-08-M5 from SMC) integrated to 3D printed manifold and controlled by a digital output module (Phidget).

Lens-Free Imaging Setup. (Supporting Figure 6) Plasmonic diffraction patterns are recorded by a lens-free imaging platform using a CMOS camera (ZWO ASI1600MM Cooled Monochrome CMOS Imaging Camera, 4/3 in. CMOS 16 MP sensor with a 4656 \times 3520 array of 3.8 μ m pixels) and \sim 823 nm laser diode source (US-Lasers Inc.). The camera is inserted in a mechanical housing designed by SolidWorks 3D CAD design software and manufactured using a 3D printer (Stratasys Eden260VS). In this imaging geometry, the distance between LED source and plasmonic chip is \sim 6 cm, and the distance between plasmonic chip and CMOS sensor array is \sim 1 cm. The housing has a dedicated space to secure the alignment of the plasmonic sensor chip and a clap to eliminate any mechanical fluctuations.

ASSOCIATED CONTENT

Supporting Information

The Supporting Information is available free of charge on the ACS Publications website at DOI: 10.1021/acssensors.7b00957.

- (i) Nearfield characteristics of the plasmonic resonances.
- (ii) Fabrication steps of the nanohole arrays.
- (iii) Multilayer structure of the flow cell.
- (iv) Complete microfluidic setup of the platform.
- (v) Spectral variation due to the attachment of polymerase.
- (vi) Lens-free sequencing platform. (PDF)

AUTHOR INFORMATION

Corresponding Author

*E-mail: acetin@omniome.com.

ORCID

Arif E. Cetin: 0000-0002-0788-8108

Author Contributions

A.E.C. conducted the research, constructed experimental setups, and collected and post-processed all data. Y.H. 3D-printed custom-made parts and manufactured the flow-cell layers. P.I. and M.W. helped with the development of the surface chemistry. A.E.C., P.I., Y.H., M.W., K.V., E.T., M.N., and A.O. wrote the paper.

Notes

The authors declare the following competing financial interest(s): The authors have a financial interest in Omniome Inc., a private company. Sequencing by Binding and SBB are trademarks of Omniome Inc.

ACKNOWLEDGMENTS

We would like to thank John Murphy for his helpful comments. We also thank UCSB Nanofabrication Facility for providing nanohole sensor chips.

REFERENCES

- (1) Nejentsev, S.; Walker, N.; Riches, D.; Egholm, M.; Todd, J. A. Rare variants of IFIH1, a gene implicated in antiviral responses, protect against type 1 diabetes. *Science* **2009**, *324*, 387–389.
- (2) Hall, J. M.; Lee, M. K.; Newman, B.; Morrow, J. E.; Anderson, L. A.; et al. Linkage of early-onset familial breast cancer to chromosome 17q21. *Science* **1990**, *250*, 1684–1689.
- (3) Grenet, O. Significance of the human genome sequence to drug discovery. *Pharmacogenomics J.* **2001**, *1*, 11–12.
- (4) Wu, L.; Candille, S. I.; Choi, Y.; Xie, D.; Jiang, L.; et al. Variation and genetic control of protein abundance in humans. *Nature* **2013**, *499*, 79–82.
- (5) Parsons, D. W.; Jones, S.; Zhang, X.; Lin, J.; Leary, R.; et al. An integrated genomic analysis of human glioblastoma multiforme. *Science* **2008**, *321*, 1807–1812.
- (6) Hastings, P. J.; Lupski, J. R.; Rosenberg, S. M.; Ira, G. Mechanisms of change in gene copy number. *Nat. Rev. Genet.* **2009**, *10*, 551–64.
- (7) Gresham, D.; Dunham, M.; Botstein, D. Comparing whole genomes using DNA microarrays. *Nat. Rev. Genet.* **2008**, *9*, 291–302.
- (8) Salgado, H.; Moreno-Hagelsieb, G.; Smith, T.; Collado-Vides, J. Operons in *Escherichia coli*: Genomic analyses and predictions. *Proc. Natl. Acad. Sci. U. S. A.* **2000**, *97*, 6652–6657.
- (9) Bentley, D. R.; Balasubramanian, S.; Swerdlow, H.; Smith, G.; Milton, J.; et al. Accurate whole human genome sequencing using reversible terminator chemistry. *Nature* **2008**, *456*, 53–59.
- (10) Shendure, J.; Porreca, G.; Reppas, N.; Lin, X.; McCutcheon, J.; et al. Accurate multiplex polony sequencing of an evolved bacterial genome. *Science* **2005**, *309*, 1728–1732.
- (11) Huang, Y. F.; Chen, S. C.; Chiang, Y. S.; Chen, T. H.; Chiu, K. P. Palindromic sequence induced sequencing-by-ligation mechanism. *BMC Syst. Biol.* **2012**, *6*, S10.
- (12) Shendure, J.; Porreca, G. J.; Reppas, N. B.; Lin, X.; McCutcheon, J. P.; et al. Accurate Multiplex Polony Sequencing of an Evolved Bacterial Genome. *Science* **2005**, *309*, 1728–1732.
- (13) Ronaghi, M.; Uhlen, M.; Nyren, P. A sequencing method based on real-time pyrophosphate. *Science* **1998**, *281*, 363–365.
- (14) Ronaghi, M.; Karamohamed, S.; Pettersson, B.; Uhlen, M.; Nyren, P. Real-time DNA sequencing using detection of pyrophosphate release. *Anal. Biochem.* **1996**, *242*, 84–89.
- (15) Rothberg, J. M.; Hinz, W.; Rearick, T.; Schultz, J.; Mileski, W.; et al. An integrated semiconductor device enabling non-optical genome sequencing. *Nature* **2011**, *475*, 348–352.
- (16) Chiosea, S. I.; Williams, L.; Griffith, C. C.; Thompson, L. D.; Weinreb, I.; et al. Molecular characterization of apocrine salivary duct carcinoma. *Am. J. Surg. Pathol.* **2015**, *39*, 744–52.
- (17) Clarke, J.; Wu, H. C.; Jayasinghe, L.; Patel, A.; Reid, S.; et al. Continuous base identification for single-molecule nanopore DNA sequencing. *Nat. Nanotechnol.* **2009**, *4*, 265–270.
- (18) Gan, H. M.; Lee, Y. P.; Austin, C. M. Nanopore Long-Read Guided Complete Genome Assembly of *Hydrogenophaga intermedia*, and Genomic Insights into 4-Aminobenzenesulfonate, p-Aminobenzoic Acid and Hydrogen Metabolism in the Genus *Hydrogenophaga*. *Front. Microbiol.* **2017**, *8*, 1880.
- (19) Shendure, J.; Ji, H. Next-generation DNA sequencing. *Nat. Biotechnol.* **2008**, *26*, 1135–1145.
- (20) Quail, M. A.; et al. A tale of three next generation sequencing platforms: comparison of Ion Torrent, Pacific Biosciences and Illumina MiSeq sequencers. *BMC Genomics* **2012**, *13*, 341.
- (21) Mckernan, K. J.; et al. Sequence and structural variation in a human genome uncovered by short-read, massively parallel ligation sequencing using two-base encoding. *Genome Res.* **2009**, *19*, 1527–1541.
- (22) Cetin, A. E.; Altug, H. Fano Resonant Ring/Disk Plasmonic Nanocavities on Conducting Substrates for Advanced Biosensing. *ACS Nano* **2012**, *6*, 9989–9995.
- (23) Joshi, G. K.; Deitz-McElyea, S.; Johnson, M.; Mali, S.; Korc, M.; et al. Highly Specific Plasmonic Biosensors for Ultrasensitive MicroRNA Detection in Plasma from Pancreatic Cancer Patients. *Nano Lett.* **2014**, *14*, 6955–6963.
- (24) Yanik, A. A.; Cetin, A. E.; Huang, M.; Artar, A.; Mousavi, S. H.; et al. Seeing Protein Monolayers with Naked Eye Through Plasmonic Fano Resonances. *Proc. Natl. Acad. Sci. U. S. A.* **2011**, *108*, 11784–11789.
- (25) Vijayan, K.; Abashin, M.; Zhang, Yi.; Kahatt, E.; Wilson, K. Sequencing device. International Patent Application WO2017117243 A1, December 28, 2016.
- (26) Zhang, W.; Huang, L.; Santschi, C.; Martin, O. J. Trapping and sensing 10 nm metal nanoparticles using plasmonic dipole antennas. *Nano Lett.* **2010**, *10*, 1006–1011.
- (27) Hao, F.; Sonnefraud, Y.; van Dorpe, P.; Maier, S. A.; Halas, N. J.; et al. Symmetry breaking in plasmonic nanocavities: subradiant LSPR sensing and a tunable Fano resonance. *Nano Lett.* **2008**, *8*, 3983–3988.
- (28) Otte, M. A.; Sepulveda, B.; Ni, W.; Juste, J. P.; Liz-Marzan, L. M.; et al. Identification of the optimal spectral region for plasmonic and nanoplasmonic sensing. *ACS Nano* **2010**, *4*, 349–357.
- (29) Shegai, T.; Johansson, P.; Langhammer, C.; Kall, M. Directional scattering and hydrogen sensing by bimetallic Pd–Au nanoantennas. *Nano Lett.* **2012**, *12*, 2464–2469.
- (30) Ebbesen, T. W.; Lezec, H. J.; Ghaemi, H. F.; Thio, T.; Wolff, P. A. Extraordinary optical transmission through sub-wavelength hole arrays. *Nature* **1998**, *391*, 667–669.
- (31) Yanik, A. A.; Huang, M.; Artar, A.; Chang, T. Y.; Altug, H. Integrated nanoplasmonic nanofluidic biosensors with targeted delivery of analytes. *Appl. Phys. Lett.* **2010**, *96*, 021101.
- (32) Cetin, A. E.; Etezadi, D.; Galarreta, B. C.; Busson, M. P.; Eksioğlu, Y.; et al. Plasmonic Nanohole Arrays on a Robust Hybrid Substrate for Highly Sensitive Label-Free Biosensing. *ACS Photonics* **2015**, *2*, 1167–1174.
- (33) Coskun, A. F.; Cetin, A. E.; Galarreta, B. C.; Alvarez, D. A.; Altug, H.; et al. Lensfree Optofluidic Plasmonic Sensor for Real-Time and Label-Free Monitoring of Molecular Binding Events over a Wide Field-of-View. *Sci. Rep.* **2017**, *4*, 6789.
- (34) Cetin, A. E.; Mertiri, A.; Erramilli, S.; Altug, H. Thermal Tuning of Surface Plasmon Polaritons Using Liquid Crystal. *Adv. Opt. Mater.* **2013**, *1*, 915–920.
- (35) Cetin, A. E.; Coskun, A. F.; Galarreta, B. C.; Huang, M.; Herman, D.; et al. Handheld High-Throughput Plasmonic Biosensor using Computational On-Chip Imaging. *Light: Sci. Appl.* **2014**, *3*, e122.
- (36) Vijayan, K.; Tu, E.; Bernard, M. A. Nucleic Acid Sequencing Methods and Systems. U.S. Patent Application 2017/0022553 A1, January 26, 2017.